Electronic Supplementary Material of

Two-dimensional Type-Ⅱ g-C_3N_4/SiP-GaS Heterojunctions as Water Splitting Photocatalysts: First-Principles Predictions

Lei Hu[a*], Wencai Yi[b], Tongde Rao[a], Jianting Tang[a], Chuanbo Hu[a], Huawei Yin[a], Haiyan Hao[a], Lei Zhang[a], Chuanjiang Li[a], and Tingzhen Li[a*]

[a] Chongqing Key Laboratory of Water Environment Evolution and Pollution Control in Three Gorges Reservoir, School of Environmental and Chemical Engineering, Chongqing Three Gorges University, Chongqing, 404100, China

[b] Laboratory of High Pressure Physics and Material Science, School of Physics and Physical Engineering, Qufu Normal University, Qufu, 273165, China

*Corresponding author**:** huleisanxu@163.com; litingzhen@163.com

ESM-1. Energetic, mechanical, dynamical and thermal stability of single-layer SiP-GaS

Firstly we calculate the cohesive energy E_{coh} of single-layer SiP-GaS using the mothed in a previous calculation[1]. The calculated E_{coh} (-5.05 eV) is more negative than that (-4.40 eV) of single-layer GaS that has been successfully synthesized in experiments[2]. Using chemical potentials, the cohesive energies of single-layer GaS-SiP and GaS are -364 and -242 meV, respectively. Briefly, single-layer SiP-GaS is even more energetically stable than synthesized GaS monolayer. Single-layer SiP-GaS belongs to C_{3V} symmetry and thus has four elastic constants, i.e. C_{11}=C_{22}, C_{12} and C_{66}. The calculated elastic constants are 110.8 N/m for C_{11}, 23.2 N/m for C_{12}, and 43.8 N/m for C_{66} respectively, satisfying the Born criterion of 2D hexagonal crystals C_{11}>0 and C_{11}-C_{12}>0.[3] Hence, monolayer SiP-GaS is mechanically stable. As shown in Figure S1(a), the phonon spectrum of monolayer SiP-GaS has no imaginary frequency, ensuring its dynamic stability. To further check the thermal stability of single-layer SiP-GaS, we perform ab-intio molecular dynamics (AIMD) simulations at 300 K for room temperature with a 6×6×1 supercell containing 144 atoms, since photocatalytic reactions usually occur at room temperature. The length of time-step is chosen as 1 fs, and 5000 steps are executed. The snapshot at the end of AIMD simulations is given in Figure S1(b), and the free energy evolution is shown in Figure S1(c). As can been seen, single-layer SiP-GaS remains a well-ordered structure at the end of AIMD simulations, proving the thermal stability of single-layer SiP-GaS.

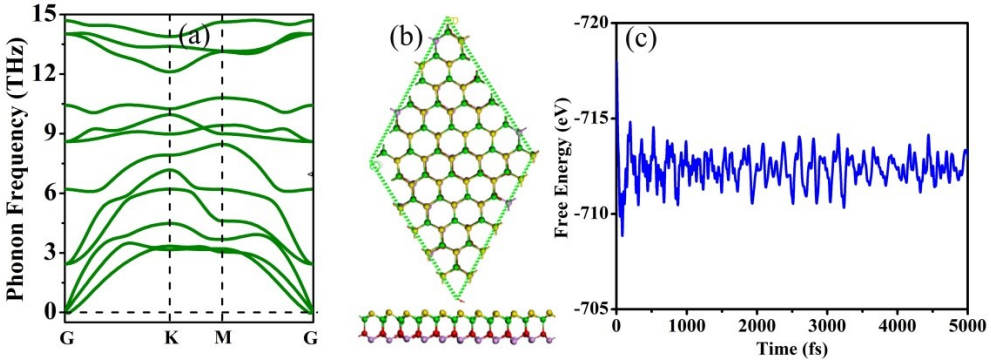

Figure S1 (a) Phonon spectrum of single-layer SiP-GaS, (b) structural snapshot of single-layer SiP-GaS at the end of AIMD simulations at 300 K, and (c) free energy variation of AIMD simulations at 300K during a timescale of 5 ps. The red, pink, green and yellow balls denote Si, P, Ga and S atoms respectively.

ESM-2. **Stability of single-layer SiP-GaS in water**

To assess the stability of 2D materials in water, one can calculate the enthalpy of solvation[4] or perform an electron localization function (ELF) analysis[5]. In the latter approach, the ELF value ranges from 0 to 1; ELF=1 corresponds to perfect localization of electrons (covalent bond) between atoms; ELF=0.5 corresponds to a homogenous electron gas (metallic bond) and ELF=0 denotes complete delocalization (no bound). The solubility can be further predicted from ELF analyses using bonding nature[6]. For instance, the strong covalent bonded g-C_2N monolayer is insoluble in water[5]. Obviously, ionic compounds embody good solubility in water. The main difference of ionic and covalent compounds is the amount of charge transfer between atoms. Ionic compounds embody good solubility in water because of large amounts of charge transfer between atoms, i.e. significant polarization of chemical bonds.

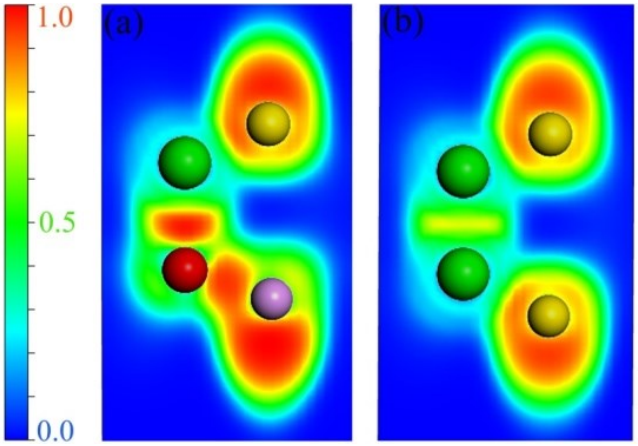

Figure S2 ELF plot along the (110) plane of monolayer (a) SiP-GaS and (b) GaS.

Here, we study the stability of monolayer SiP-GaS in water by performing an ELF analysis. The ELF plot of monolayer SiP-GaS is given in Figure S2. As can be seen in Figure S2(a), ELF~1 appears between the silicon (Si) and sulfur (S) atoms of monolayer SiP-GaS, indicating the Si-S bond exhibits covalent character. An ELF value of ~0.5 emerges around gallium (Ga) atoms, which suggests Ga-S and Ga-Si bonds present partial ionic character. As a benchmark, we also show the ELF plot of monolayer GaS that has been proven to be insoluble in water by calculating the enthalpy of solvation[4]. As discussed above, the poor solubility inherently demonstrates the covalent bond character of Ga-S bonds in single-layer GaS, even though an ELF value of ~0.5 is present around Ga atoms [cf. Figure S2(b)]. On the other side, the charge transfer from the Ga to S atom in monolayer GaS is 0.81 *e* based on Bader charge analysis. For single-layer SiP-GaS, the charge transfer from the

Ga to S atom is 0.80 *e* and smaller that in single-layer GaS. Thus, the Ga-S bond of single-layer SiP-GaS displays covalent character inherently. The electronegativity of Si element is smaller than that of sulfur element, and hence the charge transfer from the Ga to Si atom is smaller than that from the Ga to S atom, indicating the inherent covalent character of Ga-Si bonds. In brief, the Ga-S, Ga-Si and Si-P bonds in monolayer SiP-GaS all show covalent character, and therefore monolayer SiP-GaS is insoluble in water.

Additionally, a previous simulation predicts poor solubility in single-layer WS_2 though possessing partial ionic characters, which is affirmed by an experiment where WS_2 nanosheets obtained from liquid-phase exfoliation exhibit poor solubility in water[5, 7].

ESM-3. Transition between single-layer SiP-GaS and bulk SiP-GaS crystal

To examine whether single-layer SiP-GaS prefers to aggregate as 3D phase or not, we make a total energy comparison between monolayer SiP-GaS and bulk SiP-GaS crystal. As shown in Figure S3, the assumed bulk SiP-GaS crystal has a similar structure to bulk ε-GaSe crystal and contains two basic SiP-GaS layers[8]. As a benchmark, the total energies of single-layer GaS, GaSe, bulk ε-GaS and GaSe crystals are also investigated. Single-layer SiP-GaS, GaS and GaSe contain 4 atoms per unit cell, while bulk ε-SiP-GaS, ε-GaS and ε-GaSe crystals have 8 atoms per unit cell. The averaged total energy per atom $E_{tot}/atom$ of bulk ε-SiP-GaS crystal is slightly more negative than that of single-layer SiP-GaS, suggesting bulk ε-SiP-GaS crystal is more energetically stable. The more negative $E_{tot}/atom$ of bulk ε-SiP-GaS crystal, indicating it is more energetically stable than single-layer SiP-GaS.

Table S1. Comparison of total energies E_{tot} (eV) between monolayer and bulk crystals

Species	SiP-GaS	ε-SiP-GaS	GaS	ε-GaS	GaSe	ε-GaSe
E_{tot}	-20.28	-40.84	-17.76	-35.80	-16.28	-32.95
$E_{tot}/atom$	-5.07	-5.11	-4.44	-4.48	-4.07	-4.12

As shown in Figure S3(d), the phonon spectrum of bulk ε-SiP-GaS crystal shows no imaginary frequency, ensuring its dynamic stability. At the end of AIMD simulations, bulk ε-SiP-GaS crystal remains a highly ordered phase, proving its thermal stability. In brief, bulk ε-SiP-GaS crystal is

energetically, dynamically and thermally stable, so it can be synthesized in experiments. Furthermore, monolayer SiP-GaS can be synthesized via mechanical exfoliation from bulk SiP-GaS crystal. Moreover, as successful examples, single-layer GaS and GaSe have been prepared using mechanical exfoliation technique from bulk crystals[2].

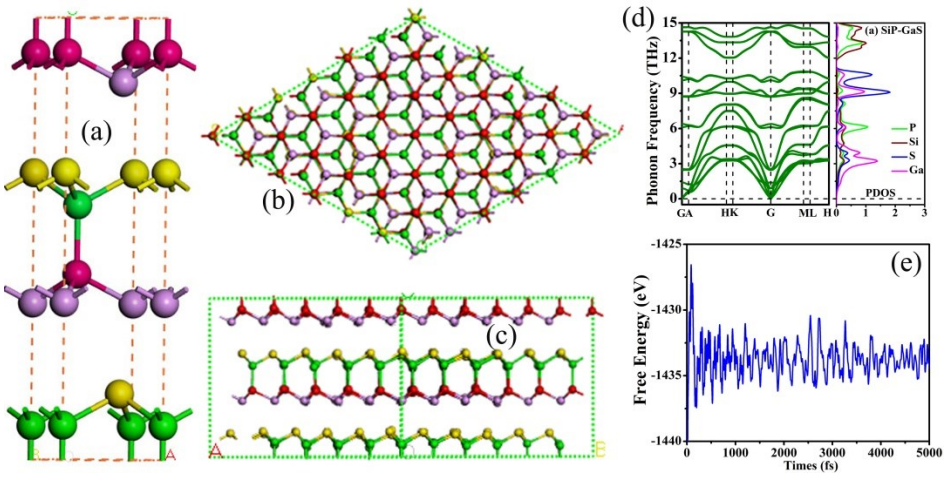

Figure S3 (a) Schematic of bulk ε-SiP-GaS crystal, (b) and (c) structural snapshot of bulk ε-SiP-GaS crystal at the end of AIMD simulations during a timescale of 5 ps. (d) Phonon band and density of states of bulk ε-SiP-GaS crystal. (e) Free energy variation of AIMD simulations.

ESM-4. Another dynamically stable 2D SiP-GaS monolayer

As shown in Figure S4(a), we find another dynamic stable 2D monolayer which is stacked in the sequence of Si-P-Ga-S. Its averaged $E_{tot}/atom$ is -4.93 eV. By contrast, the studied monolayer SiP-GaS in this main manuscript is stacked in the sequence of P-Si-Ga-S, as emphasized in Figure S4(b). The averaged $E_{tot}/atom$ of the studied monolayer in the main manuscript is more negative, indicating it is more energetically stable.

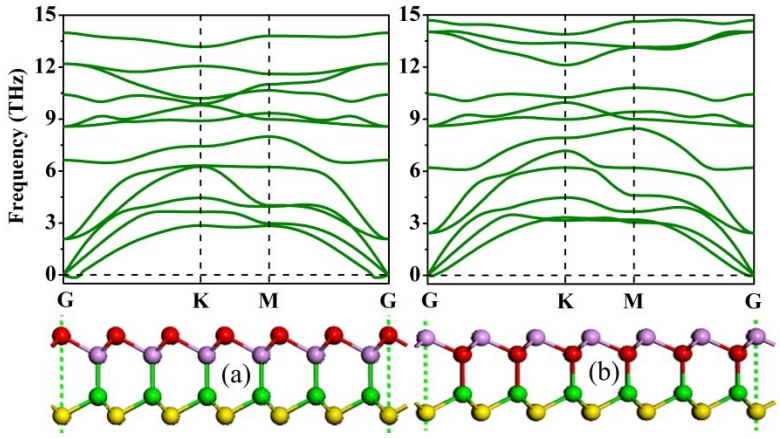

Figure S4 (a) Phonon frequency of monolayer Si-P-Ga-S. (b) That for monolayer P-Si-Ga-S. The red, pink, green and yellow balls denote Si, P, Ga and S atoms respectively.

ESM-5. Possible synthesis route and substrate to grow 2D SiP-GaS monolayer

(1) As discussed above, bulk SiP-GaS crystal is energetically, dynamically and thermally stable, indicating it can be prepared. Furthermore, the difference of averaged total energy per atom ($E_{tot}/atom$) between monolayer SiP-GaS and bulk ε-SiP-GaS crystal is very small, suggesting single-layer SiP-GaS can be synthesized via mechanical exfoliation from bulk SiP-GaS crystal.

(2) Single-layer MoSSe has been synthesized by replacing the top sulfur (S) layer with selenium (Se) atoms[9], which further indicates it is possible to synthesize monolayer SiP-GaS by replacing the GaS atomic group with the SiP atomic group.

(3) Except mechanical exfoliation, chemical vapor deposition (CVD) is another widely used method to prepare 2D materials. In the CVD method, suitable substrates that satisfy a good lattice match with desirable 2D materials are necessary[10]. To easily separate synthesized 2D materials from substrates, the interaction between 2D materials and substrates should better be the van der Waals type, e.g. graphene on metal substrates[11, 12].

Table S2. Cell sizes of monolayer SiP-GaS and substrates to achieve small lattice mismatch

Species	Pt(111)	Cu(111)	MgO(111)	Si(111)
Substrate	$3\times3\times1$	$4\times4\times1$	$3\times3\times1$	$4\times4\times1$
SiP-GaS	$2\times2\times1$	$3\times3\times1$	$\sqrt{7}\times\sqrt{7}\times1$	$3\times3\times1$
Mismatch for Substrate	+0.18%	+1.92%	+2.31%	+0.34%
Mismatch for SiP-GaS	-0.17%	-2.21%	-2.21%	-0.34%

A series of metals Ni, Pd, Pt, semiconductors Si, Ge, and insulator materials MgO and CaO could be used as substrates of 2D materials[13]. Herein, we try to apply the (111) surface of Pt, Cu, MgO and Si as substrates of monolayer SiP-GaS. To achieve small lattice mismatch, the cell sizes of the chosen substrates and monolayer SiP-GaS are given in Table S2. The Pt, Cu, MgO and Si substrates are modeled by four atomic layers, of which the bottom two layers are fixed. The optimized structures of single-layer SiP-GaS disposition on Pt (111), Cu (111), MgO (111) and Si (111)

surfaces are given Figure S5. As can be seen in Figure S5(c), single-layer SiP-GaS is destroyed on the (111) surface of MgO, so MgO (111) is not a suitable substrate to grow single-layer SiP-GaS. Single-layer SiP-GaS remains a well-ordered phase on Pt (111), MgO (111) and Si (111). The shortest bond in the interface between single-layer SiP-GaS and Pt (111) is 2.329 Å, which is shorter than the sum of the covalent radii of sulfur (S: 1.05 Å) and platinum (Pt: 1.36 Å) atoms[14]. Hence, covalent bonds exist at the SiP-GaS/Pt(111) interface. Similarly, the shortest bond (2.332 Å) at the SiP-GaS/Cu(111) interface is also shorter than the sum of the covalent radii of S (1.05 Å) and Cu (1.32 Å), indicating the existence of covalent bonds. By contrast, the shortest bond is 2.865 Å at the interface of SiP-GaS/Si(111), which is longer than the sum of the covalent radii of S (1.05 Å) and Si (1.11 Å) to some extent.

In brief, covalent bonds exist at the SiP-GaS/Pt(111) and SiP-GaS/Cu(111) interfaces, but are absent at SiP-GaS/Si(111) interface. Therefore, it is easy to transfer single-layer SiP-GaS from the Si (111) substrate. Also considering single-layer SiP-GaS remains a well-ordered phase on the (111) surface of Si, the Si (111) surface is a suitable substrate to grow single-layer SiP-GaS.

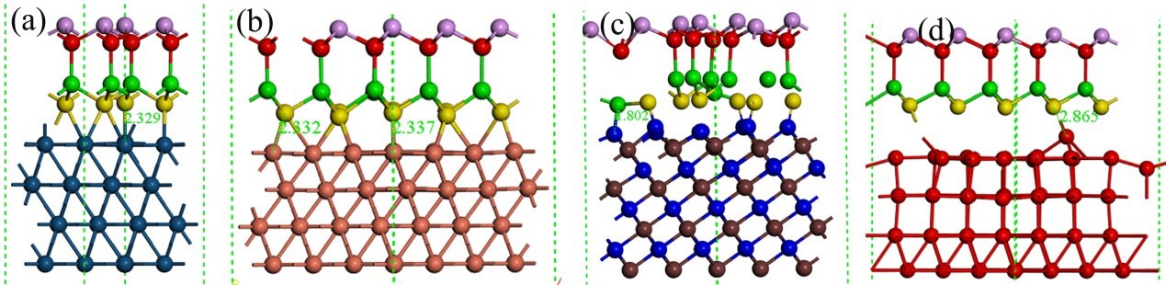

Figure S5 Schematics of monolayer SiP-GaS deposition on (a) Pt (111), (b) Cu (111), (c) MgO (111) and (d) Si (111)

ESM-6 Band edges of g-C_3N_4/SiP-GaS-α, -β and -γ at pH=5

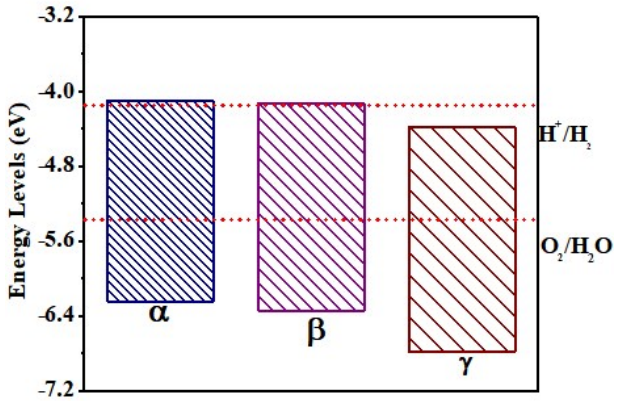

Figure S6 Band edges of g-C_3N_4/SiP-GaS-α, -β and –γ at pH=5

As can be seen, the VBM and CBM of g-C_3N_4/SiP-GaS-α and g-C_3N_4/SiP-GaS-β are also favorable to produce H_2 and O_2 at pH=5.

ESM-7 Charge transfer in g-C_3N_4/SiP-GaS-β and g-C_3N_4/SiP-GaS-γ

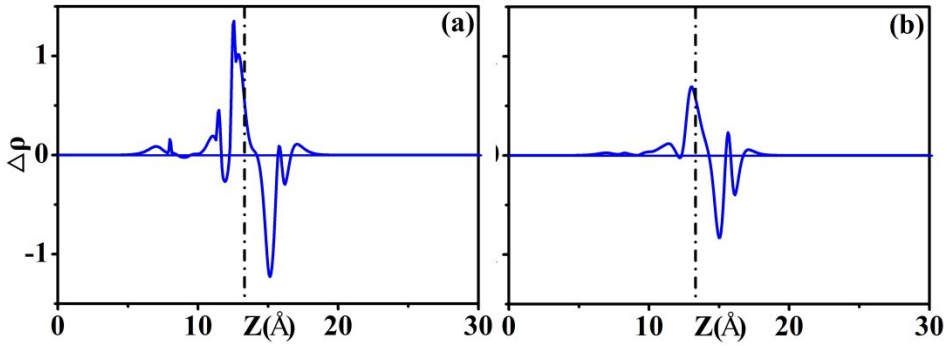

Figure S7 Charge transfer in (a) g-C_3N_4/SiP-GaS-β and g-C_3N_4/SiP-GaS-γ heterojunctions

As shown in Figure S7, a charge transfer takes place from the g-C_3N_4 layer to the SiP-GaS layer in g-C_3N_4/SiP-GaS-β and g-C_3N_4/SiP-GaS-γ heterojunctions.

ESM-8 Zero point energy (*ZPE*) and entropy (*TS*) contribution to Gibbs free energy (*G*)

Table S3. DFT energy (*E*), zero point energy (*ZPE*), entropy contribution (*TS*) and Gibbs free energy (*G*) in unit of eV for OER on the g-C_3N_4 layer

Species	*E*	*ZPE*	*TS*	*G*
OH*	-209.406	0.394	0.066	-209.078
O*	-205.072	0.093	0.040	-205.019
OOH*	-213.846	0.414	0.222	-213.654
H_2O	-14.219	0.568	0.186	-13.837
O_2	-9.844	0.099	0.124	-9.869
H_2	-6.767	0.281	0.083	-6.569
*	-199.915	0	0	-199.915

References

1. J.-H. Lin, H. Zhang, X.-L. Cheng and Y. Miyamoto, *Single-layer group IV-V and group V-IV-III-VI*

semiconductors: Structural stability, electronic structures, optical properties, and photocatalysis, *Phys. Rev. B*, 2017, **96**, 035438

2. D. J. Late, B. Liu, H. S. S. Ramakrishna Matte, C. N. R. Rao and V. P. Dravid, *Rapid Characterization of Ultrathin Layers of Chalcogenides on SiO_2/Si Substrates*, *Adv. Funct. Mater.*, 2012, **22**, 1894.
3. H. L. Zhuang, M. D. Johannes, M. N. Blonsky and R. G. Hennig, *Computational prediction and characterization of single-layer CrS_2*, *Appl. Phys. Lett.*, 2014, **104**, 022116.
4. H. L. Zhuang and R. G. Hennig, *Single-Layer Group-III Monochalcogenide Photocatalysts for Water Splitting*, *Chem. Mater.*, 2013, **25**, 3232.
5. R. Kumar, D. Das and A. K. Singh, *C_2N/WS_2 van der Waals type-II heterostructure as a promising water splitting photocatalyst*, *J. Catal.*, 2018, **359**, 143.
6. A. Mishra, P. Srivastava, H. Mizuseki, K. R. Lee and A. K. Singh, *Isolation of pristine MXene from Nb_4AlC_3 MAX phase: a first-principles study*, *Phys. Chem. Chem. Phys.*, 2016, **18**, 11073.
7. Y. Yuan, R. Li and Z. Liu, *Establishing water-soluble layered WS_2 nanosheet as a platform for biosensing*, *Anal. Chem.*, 2014, **86**, 3610.
8. L. Plucinski, R. L. Johnson, B. J. Kowalski, K. Kopalko, B. A. Orlowski, Z. D. Kovalyuk and G. V. Lashkarev, *Electronic band structure of GaSe (0001):Angle-resolved photoemission and ab initio theory*, *Phys. Rev. B*, 2003, **68**, 125304.
9. A. Y. Lu, H. Zhu, J. Xiao, C. P. Chuu, Y. Han, M. H. Chiu, C. C. Cheng, C. W. Yang, K. H. Wei, Y. Yang, Y. Wang, D. Sokaras, D. Nordlund, P. Yang, D. A. Muller, M. Y. Chou, X. Zhang and L. J. Li, *Janus monolayers of transition metal dichalcogenides*, *Nat. Nanotechnol.*, 2017, **12**, 744.
10. H. L. Zhuang, A. K. Singh and R. G. Hennig, *Computational discovery of single-layer III-V materials*, *Phys. Rev. B*, 2013, **87**, 165415.
11. G. Giovannetti, P. A. Khomyakov, G. Brocks, V. M. Karpan, J. van den Brink and P. J. Kelly, *Doping graphene with metal contacts*, *Phys. Rev. Lett.*, 2008, **101**, 026803.
12. M. Fuentes-Cabrera, M. I. Baskes, A. V. Melechko and M. L. Simpson, *Bridge structure for the graphene/Ni(111) system: A first principles study*, *Phys. Rev. B*, 2008, **77**, 035405.
13. Z. Fu, M. Liu and Z. Yang, *Substrate effects on the in-plane ferroelectric polarization of two-dimensional SnTe*, *Phys. Rev. B*, 2019, **99**, 205425.
14. B. Cordero, V. Gomez, A. E. Platero-Prats, M. Reves, J. Echeverria, E. Cremades, F. Barragan and S. Alvarez, *Covalent radii revisited*, *Dalton Trans.*, 2008, **21**, 2832.